51st AIAA Aerospace Sciences Meeting including the New Horizons Forum and Aerospace Exposition
07 - 10 January 2013, Grapevine (Dallas/Ft. Worth Region), Texas

AIAA 2013-0747

# Atmospheric Boundary Layer Studies with Unified RANS-LES and Dynamic LES Methods

Michael Stoellinger*, Harish Gopalan†, Ehsan Kazemi Foroushani‡, and Stefan Heinz§
*University of Wyoming, Laramie, WY 82071*

**The paper reports the results of applications of nonlinear dynamic LES and unified RANS-LES models to neutrally stratified atmospheric boundary layer (NABL) simulations. The advantages of dynamic LES methods are their accuracy and the ability to account correctly for anisotropy and backscatter. The advantage of unified RANS-LES models is their ability to provide results like LES for much lower computational cost. The models are applied to two flows. First, a turbulent Ekman layer with a smooth wall at the bottom is considered at a low Reynolds number $Re_f = 1140$. The results are compared with available DNS results. Second, the results of simulations of the NABL on coarse grids are presented. On coarse grids the subgrid-scale models have to provide a significant contribution, this means they are much more important than in fine grid resolution studies.**



## I. Introduction

There is a growing interest in using wind energy to provide electricity all around the globe. For example, a recent report by the Department of Energy suggests the possibility of providing 20% of the electricity in the U.S. by wind energy in 2030. A significant problem of existing wind farms is their relatively low efficiency. Due to the wind turbine wakes, the efficiency of wind farms is reduced by 20 to 50 percent compared to turbines in isolation. Therefore, there is a significant need for research related to the interaction of wind turbines with the surrounding air flow.

Numerical simulations are invaluable for obtaining a comprehensive understanding of wind farm processes. However, such simulations face significant problems related to the consistency of equations, the generality of equations, and the computational cost of simulations. A very promising approach to find general solutions for these questions is the development of turbulence models on the basis of stochastic analysis. Unified combinations of Reynolds-averaged Navier-Stokes (RANS) equations with large eddy simulation (LES) equations and dynamic LES equations were presented recently by Heinz.[1,2] The advantages of dynamic LES methods are their accuracy and the ability to account correctly for anisotropy and backscatter. The advantage of unified RANS-LES models is their ability to provide results like LES for much lower computational cost. Details about the characteristic features of these methods and applications to channel flow simulations can be found elsewhere.[3–5]

The purpose of this paper is to report applications of these unified and dynamic methods to turbulent boundary-layer turbulence studies relevant to wind energy applications. The turbulence models applied will be described in section II. Section III briefly presents the flows considered and the numerical method applied. The results obtained by unified and dynamic LES models are discussed in section IV. Section V summarizes the conclusions of these studies.

*Assistant Professor, Department of Mechanical Engineering, 1000 E. University Avenue, Laramie WY 82071.
†Post Doctoral Research Associate, Department of Mechanical Engineering, 1000 E. University Avenue, Laramie WY 82071.
‡PhD student, Department of Mathematics, 1000 E. University Avenue, Laramie WY 82071.
§Associate Professor, Department of Mathematics, 1000 E. University Avenue, Laramie WY 82071, Email: heinz@uwyo.edu, Senior Member AIAA

## II. Unified and Dynamic Model Equations

For the incompressible flow considered here the LES equations for filtered velocities $\overline{U}_i$ $(i = 1, 2, 3)$ are given by the incompressibility constraint

$$\partial \overline{U}_i / \partial x_i = 0, \tag{1}$$

and the momentum equations for a rotating reference frame

$$\frac{\overline{D}\,\overline{U}_i}{\overline{D}t} = -2\varepsilon_{ijk}\Omega_j \overline{U}_k - \frac{\partial \overline{P}}{\partial x_i} + 2\nu \frac{\partial \overline{S}_{ik}}{\partial x_k} - \frac{\partial \tau^d_{ik}}{\partial x_k}. \tag{2}$$

Here, $\varepsilon_{ijk}$ is the permutation tensor and $\Omega_j$ is the rotation vector. The filtered Lagrangian time derivative is denoted by $\overline{D}/\overline{D}t = \partial/\partial t + \overline{U}_k\,\partial/\partial x_k$ , $\overline{P} = \overline{p}/\rho + \frac{2}{3}k$ is the modified filtered pressure, $k$ is the subgrid-scale (SGS) kinetic energy, $\rho$ is the constant fluid mass density, $\nu$ is the constant kinematic viscosity, $\tau^d_{ij}$ is the deviatoric part of SGS stress tensor, and $\overline{S}_{ij} = (\partial \overline{U}_i/\partial x_j + \partial \overline{U}_j/\partial x_i)/2$ is the rate-of-strain tensor. The sum convention is used throughout this paper. Different models for the SGS stress tensor $\tau^d_{ik}$ are used in this work. The different models are all based on a quadratic (in the shear) approximation of the form[1,2]

$$\tau^d_{ij} = -2\nu_{sgs}\overline{S}_{ij} - 3\frac{\nu^2_{sgs}}{k}\left[\overline{S}_{ik}\overline{\Omega}_{kj} + \overline{S}_{jk}\overline{\Omega}_{ki} - 2\overline{S}_{ik}\overline{S}_{kj} + \frac{2}{3}\overline{S}_{nk}\overline{S}_{kn}\delta_{ij}\right], \tag{3}$$

where $\overline{\Omega}_{ij} = (\partial \overline{U}_i/\partial x_j - \partial \overline{U}_j/\partial x_i)/2$ is the rate-of-rotation tensor. An additional transport equation for the SGS kinetic energy $k$ is solved. The filter width $\Delta$ that appears in the SGS models is related to the computational grid by $\Delta = (\delta_x \cdot \delta_y \cdot \delta_z)^{1/3}$.

### A. Dynamic model

A dynamic nonlinear SGS model is given by[2]

$$\tau^d_{ij} = -2\nu_{sgs}\overline{S}_{ij} - C_n\Delta^2\left[\overline{S}_{ik}\overline{\Omega}_{kj} + \overline{S}_{jk}\overline{\Omega}_{ki} - 2\overline{S}_{ik}\overline{S}_{kj} + \frac{2}{3}\overline{S}_{nk}\overline{S}_{kn}\delta_{ij}\right], \tag{4}$$

with the SGS viscosity defined as

$$\nu_{sgs} = C_k \Delta k^{1/2}. \tag{5}$$

The two model coefficients $C_k$ and $C_n$ are calculated from a dynamic procedure based on an explicit test filter with a test filter width of $\widetilde{\Delta} = 2\Delta$. No averaging of the dynamic model coefficients is applied. To ensure numerical stability the calculated values are bounded by $-0.2 < C_k < 2$ and $-1 < C_n < 2$. The evolution of the SGS kinetic energy is given by

$$\frac{\overline{D}k}{\overline{D}t} = \frac{\partial}{\partial x_k}\left[(\nu + \nu_{sgs})\frac{\partial k}{\partial x_k}\right] - \tau^d_{ij}\frac{\partial \overline{U}_j}{\partial x_i} - \frac{k^{3/2}}{\Delta}. \tag{6}$$

When the dynamic model is used in simulations with a smooth wall and near wall resolution a no-slip boundary condition and $k = 0$ are used at the wall. For cases where the dynamic model is applied in coarse grid simulations with a rough wall based on a roughness height $z_0$, the no-slip boundary condition is not warranted. For these simulations, the shear stress at the wall is directly imposed using the method of Schumann[6]

$$\tau_{i3_w} = -u_* \frac{\overline{U}_i(x, y, z_p)}{S(z_p)}, \tag{7}$$

where $z_p$ denotes the center of the first cell adjacent to the wall, $S(z_p)$ is the magnitude of the horizontally averaged velocity vector and the friction velocity $u_*$ is obtained from

$$u_* = \kappa \frac{S(z_p)}{log(z_p/z_0)}, \tag{8}$$

with $\kappa = 0.41$. The velocity normal to the surface is set to be zero and a zero gradient condition is specified for $k$.

## B. Smooth wall unified LES-RANS model

In the unified RANS-LES model the expression for the modeled stress tensor is given by

$$\tau_{ij}^d = -2\nu_t \overline{S}_{ij} - 3\frac{\nu_t^2}{k}\left[\overline{S}_{ik}\overline{\Omega}_{kj} + \overline{S}_{jk}\overline{\Omega}_{ki} - 2\overline{S}_{ik}\overline{S}_{kj} + \frac{2}{3}\overline{S}_{nk}\overline{S}_{kn}\delta_{ij}\right]. \tag{9}$$

The modeled turbulent viscosity $\nu_t$ is related to the relevant length scale of turbulent motions $L_m$ and the turbulent kinetic energy,

$$\nu_t = C_k^* L_m \sqrt{k}. \tag{10}$$

The parameter $C_k^*$ is given below. The relevant length scale is determined from $L_m = min(\Delta, L)$ where $L$ is the integral length scale (the scale of the largest turbulent motions). Therefore, the unified model provides a smooth transition between the eddy viscosity in the RANS regime and in the LES regime,

$$\nu_t = \begin{array}{ll} C_k^* L\sqrt{k} & \text{RANS regime: } \Delta \geq L \\ C_k^* \Delta\sqrt{k} & \text{LES regime: } \Delta < L. \end{array} \tag{11}$$

The integral length scale is calculated as $L = \sqrt{k}/\omega$ where the turbulent frequency $\omega$ is obtained from the transport equation[7]

$$\frac{\overline{D}\omega}{\overline{D}t} = C_{\omega 1}\frac{\omega}{k}P - \frac{C_{\omega 2}}{C_k}\omega^2 + \frac{\partial}{\partial x_j}\left[(\nu + \frac{\nu_t}{\sigma_\omega})\frac{\partial \omega}{\partial x_j}\right] + \frac{c_\omega}{k}(\nu + \nu_t)\frac{\partial k}{\partial x_j}\frac{\partial \omega}{\partial x_j}, \tag{12}$$

where $C_k = 0.09$, $C_{\omega 1} = 0.49$, $C_{\omega 2} = 0.072$, $C_\omega = 1.1$, and $\sigma_\omega = 1.8$. The production of modeled kinetic energy P is given by $P = -\tau_{ij}^d \partial \overline{U}_i/\partial x_j$. The $\omega$ equation can be either used by integrating through the viscous region or by placing the first grid point into the log-layer. This is achieved by specifying the value at the first grid point above the wall by the expression[8]

$$\omega = \sqrt{\left(\frac{2\nu}{d_y^2}\right)^2 + \left(\frac{\sqrt{k}C_k^{0.75}}{\kappa d_y}\right)^2}. \tag{13}$$

To account for the wall damping on the turbulent viscosity the constant $C_k$ is modified by a damping function $f_\mu$ to give $C_k^* = C_k f_\mu$ with

$$f_\mu = 0.09 + \left(0.91 + \frac{1}{Re_t^3}\right)(1 - e^{-\left(\frac{Re_t}{25}\right)^{2.75}}), \tag{14}$$

where $Re_t = C_k k/(\omega\nu)$. The modeled kinetic energy is obtained from the solution of the equation

$$\frac{\overline{D}k}{\overline{D}t} = \frac{\partial}{\partial x_k}\left[(\nu + \nu_t)\frac{\partial k}{\partial x_k}\right] + P - \frac{k^{3/2}}{L_m}. \tag{15}$$

No-slip and $k = 0$ boundary conditions are applied at the wall.

## C. Rough wall unified LES-RANS model

The simulations of the neutral atmospheric boundary layer (NABL) require a different wall law based on the surface roughness parameter $z_0$. In RANS simulations of the ABL the $k - \varepsilon$ model is often applied.[9] Therefore, the integral length scale in the unified model for the NABL is based on the dissipation of turbulent kinetic energy $L = k^{3/2}/\varepsilon$. The dissipation rate is determined via the modeled transport equation

$$\frac{\overline{D}\epsilon}{\overline{D}t} = C_1\frac{\epsilon}{k}P - C_2\frac{\epsilon^2}{k} + \frac{\partial}{\partial x_k}\left[(\nu + \nu_t/\sigma_e)\frac{\partial k}{\partial x_k}\right], \tag{16}$$

where $C_1 = 1.44$, $C_2 = 1.92$ and $\sigma_e = 1.3$. The dissipation at the first cell off the wall is set to $\varepsilon(z_p) = C_k^{0.75} k(z_p)^{1.5}/(\kappa z_p)$, and the production term is calculated from $P = -\tau_{13_w}\partial\overline{U}_1/\partial z - \tau_{23_w}\partial\overline{U}_2/\partial z$. A zero gradient boundary condition is applied for $k$.

**Table 1. Parameters for the Ekman layer.**

| Parameters | Value |
|---|---|
| Reynolds number $Re_f = U_g L_z/\nu$ | 1141 |
| Ekman layer height $\delta_e$ | 1 |
| Rossby number $Ro = U_g/(fL_z)$ | 10 |
| Domain size | $L_x = 2\delta_e$, $L_y = 2\delta_e$, $L_z = 2\delta_e$ |

## III. Test cases considered and numerical method

To evaluate the performance of the SGS models presented above we consider two test cases. First, a turbulent Ekman layer with a smooth wall at the bottom is investigated at a low Reynolds number $Re_f = 1140$. The reason for considering this flow is the availability of a high quality DNS database[10] provided by the Kawamura Lab (http://murasun.me.noda.tus.ac.jp/turbulence/), which can be used for the model validation. The geostrophic wind $U_g$ is in streamwise ($x$) direction. The wall normal direction is $z$ and the rotation is around the wall normal direction with $\mathbf{\Omega} = (0, 0, f/2)$, where $f$ is the Coriolis parameter. The relevant parameters are summarized in table 1. Three different grids are considered: a fine grid (GF) suitable for LES up to the wall (i.e. without near wall model), a coarser grid *GC* with half the points in streamwise and spanwise directions but a comparable resolution in the wall normal direction, and a very coarse grid (GVC) used to test the performance of the unified model. The details of the three grids are listed in table 2.

The second test-case is the neutrally stratified ABL with $U_g = 10m/s$, $\mathbf{\Omega} = (0, 0.0005, 0.005)$ and a roughness height $z_0 = 0.1m$. The NABL simulations are performed on a domain of $L_x = 4km$, $L_y = 3km$, $L_z = 1.5km$. A fine equidistant grid of $N_x = N_y = N_z = 80$ is used for the dynamic model simulation. The unified model simulation is performed on a $N_x = N_y = N_z = 50$ grid with stretching in the z-direction.

Simulations were performed by using a finite-volume based method inside the OpenFOAM CFD Toolbox. In all simulation the geostrophic wind is used to drive the neutral boundary layer simulations. The convection term in the momentum equation was discretized using a second-order central difference scheme. The PISO algorithm was used for the pressure-velocity coupling. The resulting algebraic equation for all the flow variables except pressure has been solved iteratively using a preconditioned bi conjugate gradient method with a diagonally incomplete LU preconditioning at each time step. The Poisson equation for the pressure was solved using an algebraic multi-grid (AMG) solver. When the scaled residual became less than $10^{-6}$, the algebraic equation was considered to be converged. Time marching was performed using a second-order Cranck-Nicholson scheme. The time step was modified dynamically to ensure a constant CFL number of 0.5. Periodic boundary conditions have been employed along the streamwise and spanwise directions for all the flow variables. At the top boundary a slip-wall condition was specified for the velocity and zero gradient conditions for all other variables.

All simulations have been initialized with the mean geostrophic wind $U_g$. Random perturbations drawn from a Gaussian distribution with zero mean and a variance of $(U_g/20)^2$ are superimposed to ease the transition to a turbulent state. All simulations are run for a time of $t_f = 3/f$ before averaging is started. Time averaging is then performed for a time period of $t_f$. The time averages are additionally averaged over the homogeneous directions.

**Table 2. Grids used in the simulations of the Ekman layer.**

| Grid | $N_x \times N_y \times N_z$ | $z_p^+$, $\delta_z^+$, $\delta_x^+$, $\delta_y^+$ |
|---|---|---|
| GF | $120 \times 120 \times 120$ | 2.9, 6, 29, 29 |
| GC | $48 \times 48 \times 96$ | 3, 6.2, 73, 73 |
| GVC | $48 \times 48 \times 48$ | 17, 34.4, 73, 73 |

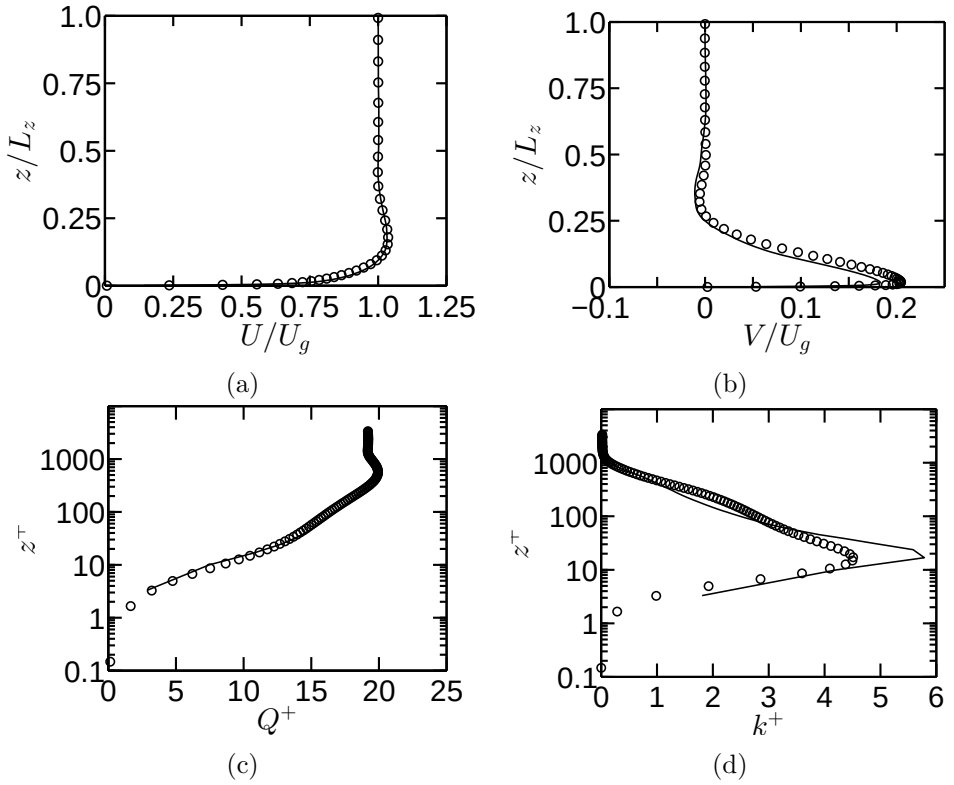


**Figure 1. Results of the dynamic LES Ekman layer simulation (lines) compared with DNS results (circles). (a) Normalized streamwise velocity, (b) normalized spanwise velocity, (c) mean wind profile in wall units, (d) turbulent kinetic energy in wall units.**

## IV. Results and Discussion

The results for the Ekman layer are discussed first. Figure 1 shows results of the dynamic model simulation using the GF grid in comparison to the DNS data. The mean streamwise and spanwise velocities are predicted well. The mean wind $Q = \sqrt{U^2 + V^2}$ is plotted in 1 (c) using wall scaling. The simulations agree well with the DNS data and and a log-law region can be identified. The profile of the turbulent kinetic energy (resolved plus modeled) is shown in (d) using wall scaling. The simulation results do qualitatively agree but a slight over prediction of the peak value can be observed. We believe this over prediction is a consequence of the low order numerical method that is used. Using an even finer resolution would be required to remove this over prediction, but this was not attempted. Overall, the use of the dynamic model on a grid that is able to resolve the near wall structures provides results in a very good agreement with DNS data.

The results of simulations performed with the unified RANS-LES model are shown in figure 2 for the GC and GVC grids. Regarding the GC simulation, the results for the mean velocities in (a) and (b) agree well with the DNS data. The GVC simulation results display a more pronounced difference to the DNS results. In particular, the spanwise velocity decays too fast. The results for the mean wind in wall scaling, see Fig. 2(c), show that the GC simulation results agree very well with the DNS data in the buffer layer. There is, however, a small mismatch in the logarithmic layer. The location of the mismatch coincides with the transition from RANS to LES at $z^+ \approx 20$. The transition happens to be located right around the peak of the turbulent kinetic energy. It has previously been shown[3] that the unified model performs better when the transition region is placed away from the turbulent kinetic energy peak. Indeed, the GVC grid simulation captures the initial log-law region quite well, but there is some disagreement further away from the wall. Most likely, this disagreement is caused by an insufficient grid resolution. The structure of the Ekman layer requires a sufficient number of grid points to be placed within the Ekman layer depth $\delta_E/L_Z = 0.04$. This requirement is somewhat conflicting with the requirement to have the RANS-LES transition region sufficiently far away from the wall. One possible remedy would be to further decrease the resolution in the streamwise and spanwise direction. However, this would likely lead to a reduced accuracy in the LES region.

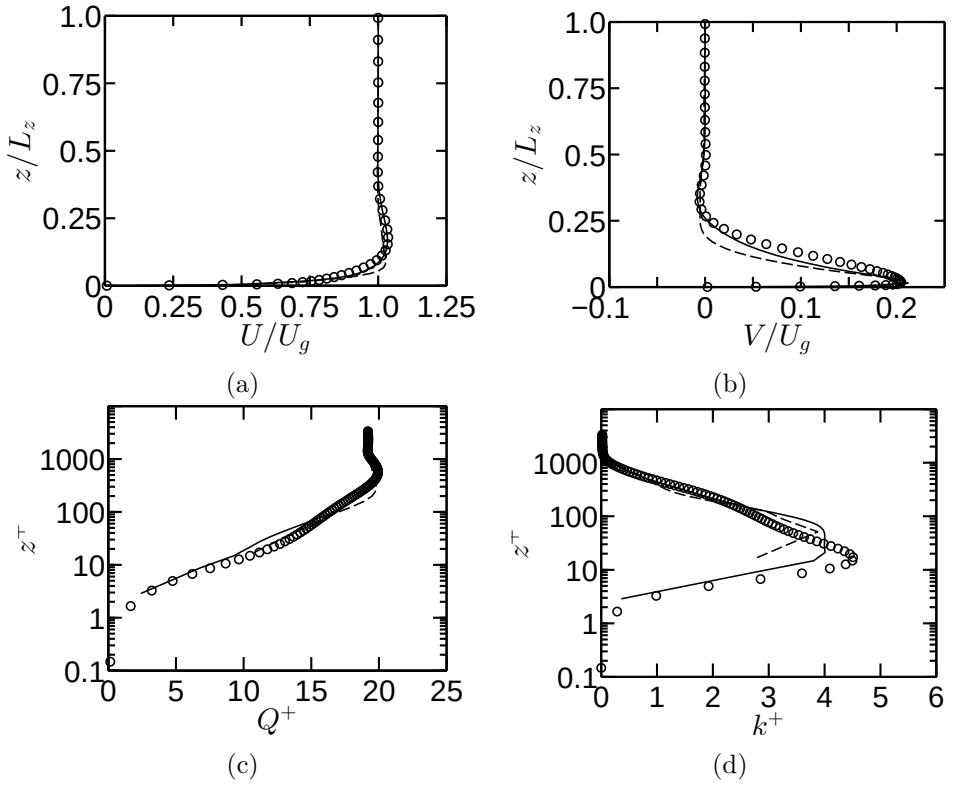


**Figure 2. Results of the unified LES-RANS Ekman layer simulations on the GC grid (solid line) and GVC grid (dashed line) in comparison to DNS results (circles). (a) Normalized streamwise velocity, (b) normalized spanwise velocity, (c) mean wind profile in wall units, (d) turbulent kinetic energy in wall units.**



A better solution might be obtained by defining the transition from RANS to LES to occur at say $\Delta < L/2$. This would place the transition further away from the wall without reducing the accuracy of the LES region results.

The difference in the structural content between the well resolved GF dynamic LES and the coarser GC unified LES-RANS simulation can be visualized by contours of the instantaneous streamwise velocity in planes normal to the wall. Figure 3 shows results at $z^+ = 30$ (top) and $z^+ = 100$ (bottom) for the dynamic (left) and unified (right) models. The long elongated structures of boundary layer turbulence are clearly visible in both model predictions at $z^+ = 30$. However, the dynamic model results display much finer structures due to the higher resolution and the inclusion of backscatter effects.[5] Further away from the wall at $z^+ = 100$ the structures become less organized and more isotropic.

The simulation results for the neutrally stratified boundary layer are presented next. Figure 4 shows a comparison between the results obtained with the dynamic model and the unified LES-RANS model. The unified model predicts a slightly smaller increase of the mean wind speed with the height than the dynamic model, as can be seen in plot (a). Plot (b) shows the mean wind using surface layer scaling $Q^+ = Q/u_*$ and $z^+ = z/z_0$. The dynamic model results follow the log-law $u_*/\kappa \cdot log(z/z_0)$ closer than the unified model results. The normalized mean velocity gradient

$$\Phi_m = \frac{\kappa z}{u_*}\sqrt{\frac{\partial\langle\overline{U}\rangle}{\partial z} + \frac{\partial\langle\overline{V}\rangle}{\partial z}} \tag{17}$$

is shown in plot (c). The dynamic model predicts values larger than the theoretical value $\Phi_M = 1$ and displays significant fluctuations. One reason for the fluctuations could be that the time averaging period was not sufficiently long. Instantaneous gradients have been averaged in the calculation of $\Phi_M$. Using the gradients of the averaged velocity should lead to smoother results. The large $\Phi_M$ values predicted by the dynamic model indicate that the chosen grid was too coarse to be in the high accuracy zone as defined by Brasseur and Wei.[11] Even though the grid used in the dynamic simulation was finer than in previous

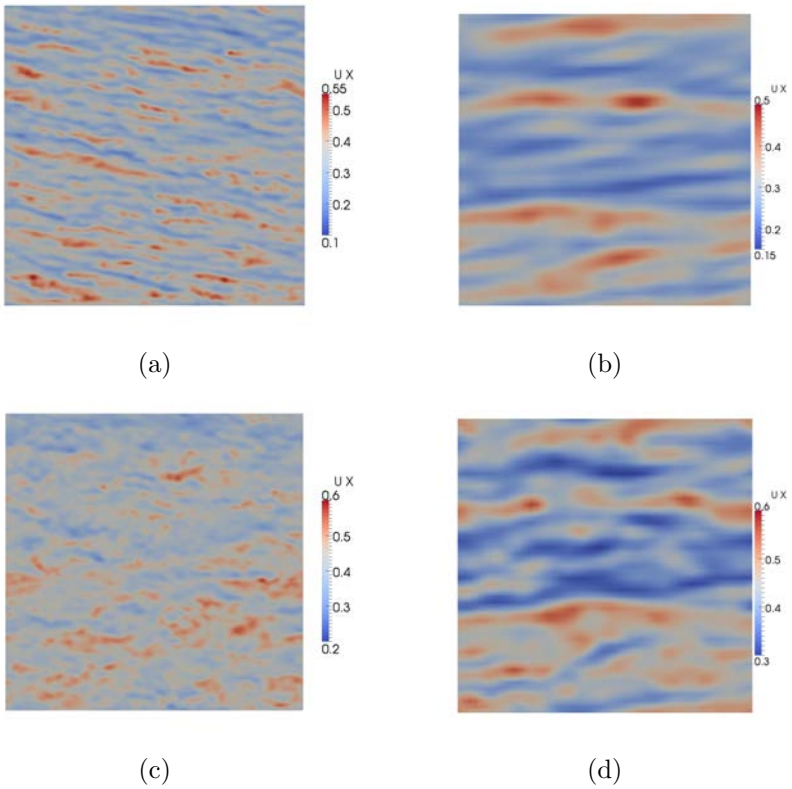


**Figure 3. Instantaneous streamwise velocity contour plots obtained for the Ekman layer. (a) dynamic model at $z^+ = 30$, (b) unified model GC at $z^+ = 30$, (c) dynamic model at $z^+ = 100$, (d) unified model GC at $z^+ = 100$.**

studies,[12,13] our numerical method is only second order accurate as compared to the more widely used spectral discretization. The unified model stays close to the theoretical value $\Phi_M = 1$ above the surface even on the coarse grid that has been used. This shows that the use of the unified LES-RANS model is preferable in low resolution simulations of the ABL.

In a typical low resolution LES of the ABL the SGS stress contributes significantly to the total stresses. Near the surface, the total normal stresses are known to be highly anisotropic. The SGS stress model should be able to capture anisotropies. The quadratic SGS stress model used in this work is able to predict anisotropic normal stresses, as can be seen from Figure 5. With regard to both models, the streamwise normal stress component $\tau_{xx}$ is significantly larger than the $\tau_{yy}$ and $\tau_{zz}$ components.

The modeled, resolved and total shear stress $\tau_s = \sqrt{\tau_{xz}^2 + \tau_{yz}^2}$ is shown in Figure 6 for the dynamic (left) and unified (right) models. Overall, the unified model predicts a much larger total shear stress. The reason for the larger total shear stress predicted by the unified model is that the grid was stretched in the wall normal direction leading to a first cell center being closer to the surface than in the dynamic model simulations. In LES, the resolved stress should contribute more than 80% to the total stress. This behavior is correctly shown by the dynamic simulation, which is attributed to the inclusion of backscatter which transfers kinetic energy from the modeled to the resolved scales.[14,15] The resolved shear stress predicted by the unified model is smaller than the modeled shear stress close to the surface. This behavior is expected since the near surface region operates in a RANS mode and hence the modeled contribution has to be larger than the resolved contribution. It should be noted that the switch between RANS and LES is predicted around $z/L_z \approx 0.1$, which is also the location where the resolved shear stress becomes larger than the modeled shear stress.

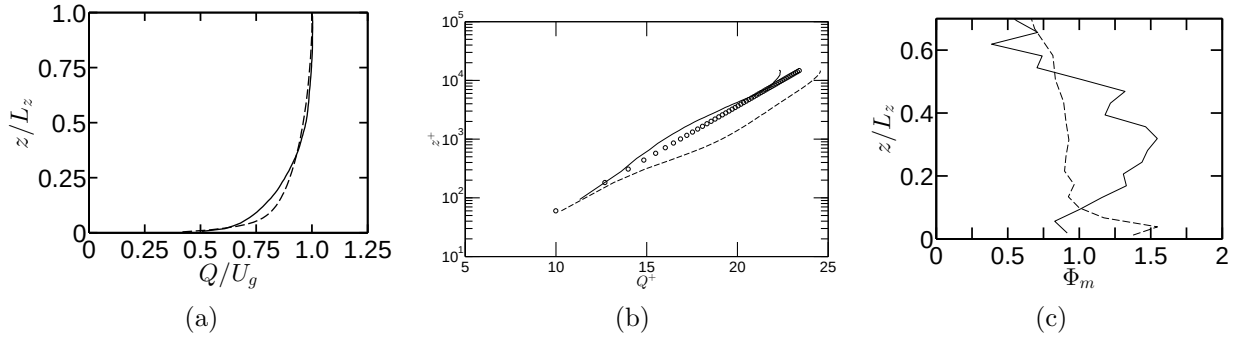


**Figure 4. Results of the NABL simulations using the dynamic model (solid line) and the unified model (dashed line). (a) mean wind profile, (b) log-law scaling, (c) normalized mean gradient.**



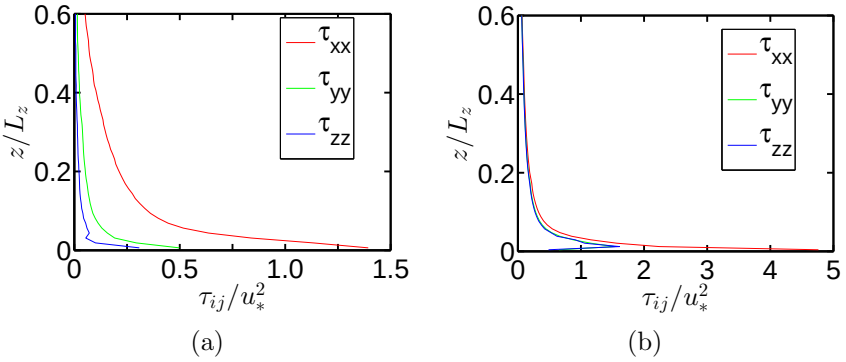


**Figure 5. SGS normal stress predictions (a) dynamic model, (b) unified model.**

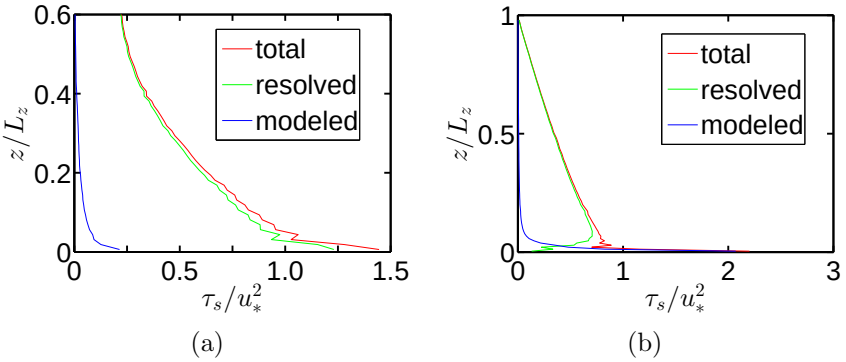


**Figure 6. Shear stress predictions (a) dynamic model, (b) unified model.**

## V. Conclusions

The paper reports the results of applications of dynamic LES and unified RANS-LES models to ABL simulations. The purpose of developing dynamic LES methods is to develop an accurate but computationally feasible methodology that can be used for the validation of simpler methods (like unified RANS-LES models) for high Reynolds number flows. The purpose of developing unified RANS-LES models is to develop a methodology that can be used for providing computationally efficient but accurate predictions of large-scale problems like the ABL.

The dynamic SGS model is found to perform very well when applied in simulations with a high resolution. The model's ability to accurately account for anisotropy and backscatter are the main reasons for the good performance. Pictures of instantaneous streamwise velocities reveal that the dynamic model is capable of representing the small-scale structure of turbulence very well. More studies on the effects of the numerical method and the grid resolution are required to assess the model performance in simulations with a fairly coarse resolution.

The unified RANS-LES model performed reasonably well in both the simulations of the Ekman layer at a low Reynolds number and the NABL. Since less resolution is required, the unified model provides computationally efficient simulations. The application of unified RANS-LES methods represents a very attractive alternative to the use of coarse LES, which is often applied in ABL simulations. The question of how the location of the transition between RANS and LES regimes affects the accuracy of model predictions needs further investigations.



## Acknowledgments

The authors would like to acknowledge support for this work through a gift from BP Alternative Energy North America Inc to the UW Wind Energy Research Center. Support from the UW School of Energy Resources providing graduate assistantship for E. Kazemi Foroushani is gratefully acknowledged. This work was partially supported by the UW Institute for Scientific Computation.

## References

[1]Heinz, S., "Unified turbulence models for LES and RANS, FDF and PDF simulations," *Theoretical and Computational Fluid Dynamics*, Vol. 21, No. 2, 2007, pp. 99–118.

[2]Heinz, S., "Realizability of dynamic subgrid-scale stress models via stochastic analysis," *Monte Carlo Methods and Applications*, Vol. 14, No. 4, 2008, pp. 311–329.

[3]Heinz, S., Gopalan, H., and Stöllinger, M., "A unified RANS-LES model. Part 1. Computational model development," *Journal of Computational Physics*, Vol. 231, 2012, pp. submitted.

[4]Gopalan, H., Heinz, S., and Stöllinger, M., "A unified RANS-LES model. Part 2. Model accuracy and computational cost," *Journal of Computational Physics*, Vol. 231, 2012, pp. submitted.

[5]Heinz, S. and Gopalan, H., "Realizable Versus Non-Realizable Dynamic Sub-Grid Scale Stress Models," *Physics of Fluids*, Vol. 24, No. 11, 2012, pp. 115105/1–23.

[6]Schumann, U., "Sugrid-scale model for finite difference simulation of turbulent flows in plane channels and annuli," *Journal of Computational Physics*, Vol. 18, 1975, pp. 376–404.

[7]Davidson, L. and Peng, S., "Hybrid LES-RANS modelling: a one-equation SGS model combined with a k-$\omega$ model for predicting recirculating flows," *International Journal for Numerical Methods in Fluids*, Vol. 43, No. 9, 2003.

[8]Wilcox, D., "Turbulence modeling for CFD, DCW Industries," *Inc., La Canada, California*, Vol. 91011, 1998.

[9]Bechmann, A. and Sørensen, N. N., "Hybrid RANS/LES applied to complex terrain," *Wind Energy*, Vol. 14, 2011, pp. 225–237.

[10]Shingai, K. and Kawamura, H., "Direct numerical simulation of turbulent heat transfer in the stably stratified Ekman layer," *Thermal Science and Engineering*, Vol. 10, No. 1, 2002, pp. 25–33.

[11]Brasseur, J. G. and Wei, T., "Designing large-eddy simulation of the turbulent boundary layer to capture law-of-the-wall scaling," *Physics of Fluids*, Vol. 22, No. 021303, 2010, pp. 1–21.

[12]Andren, A., Brown, A. R., Mason, P. J., Graf, J., Schumann, U., Moeng, C. H., and Nieuwstadt, F. T. M., "Large-eddy simulation of a neutrally stratified boundary layer: A comparison of four computer codes," *Quarterly Journal of the Royal Meteorological Society*, Vol. 120, No. 520, 1994, pp. 1457–1484.

[13]Anderson, W. C., Basu, S., and Letchford, C. W., "Comparison of dynamic subgrid-scale models for simulations of neutrally buoyant shear-driven atmospheric boundary layer flows," *Environmental Fluid Mechanics*, Vol. 7, No. 3, 2007, pp. 195–215.

[14]Sullivan, P. P., McWilliams, J. C., and Moeng, C. H., "A subgrid-scale model for large-eddy simulation of planetary boundary-layer flows," *Boundary-Layer Meteorology*, Vol. 71, No. 3, 1994, pp. 247–276.

[15]Kosović, B., "Subgrid-scale modelling for the large-eddy simulation of high-Reynolds-number boundary layers," *Journal of Fluid Mechanics*, Vol. 336, No. 1, 1997, pp. 151–182.